ISES International Solar Energy Society

Conference Proceedings

EuroSun 2014
Aix-les-Bains (France), 16 - 19 September 2014

Numerical and Experimental Approaches for the Characterization of Heat Transfer Mechanisms in Compound Parabolic Concentrators

Christoph Reichl[1], Florian Hengstberger[1], Christoph Zauner[1] and Bernhard Kubicek[1]

[1] Austrian Institute of Technology, Energy Department, Vienna (Austria)

Abstract

Several physical mechanisms including conduction, convection, diffusion and radiation are involved when modelling heat transfer in a solar collector. A lab scale compound parabolic concentrator collector model was first analysed by particle image velocimetry (PIV) and local temperature probes for various tilt angles of the setup and different absorber tube temperatures to provide a base for comparison to computational fluid dynamics (CFD) results. To be able to separate the occurring effects no incoming radiation was used for the measurements: To drive the convective flow inside the CPC, the absorber temperature was fixed to a constant temperature instead. The Navier Stokes equations have been solved on 2D and 3D meshes using steady and transient solutions: for a detailed reproduction of the experimentally observed natural convection currents transient 3D approaches are required – if only overall temperatures, approximate velocity ranges and heat fluxes are of primary interest, computationally cheap two dimensional steady approaches can be facilitated. These simulations can also be used for a fast assessment of efficiency curves in various scenarios. Ray-tracing is utilized to describe the solar radiation patterns and investigate the influence of distributed energy sources on tube and mirror.

Keywords: CPC collector, Ray-tracing, Particle Image Velocimetry (PIV), Computational Fluid Dynamics (CFD), heat transfer mechanisms, solar radiation

1. Introduction

Hot absorber surface-areas being an important source of heat loss can be significantly reduced by introducing the concept of parabolic solar concentrators, which however have to be tracked to stay in the focus of the incoming solar radiation. Presenting moderate concentration ratios, CPCs - Compound Parabolic Concentrators (Buttinger et. al., 2010; Horta et al., 2012) combine some of the advantages of the stationary solar collector with the reduced hot absorber surface due to the concentration of solar radiation. CPCs show an acceptance angle for the incoming solar radiation and thus have not to be tracked. Heat transfer mechanisms can be partly described by empirical correlations (Singh and Eames, 2011) and natural convection currents in CPCs prompted noticeable interest (Horta et al., 2012, ; Eames and Norton, 2010, Khonkar et. al. (1995), Chew et. al., 1989 and Abdel-Khalik and Randell, 1978).

In this contribution we will compare numerical simulations (CFD) with results from particle image velocimetry (PIV) and local temperature measurements and extend previous studies (Reichl et. al., 2013) with ray-tracing techniques. For this purpose a lab scale compound parabolic concentrator collector model was analysed by particle image velocimetry (PIV) and local temperature probes for various absorber tube temperatures and tilt angles. For these measurements, no incoming radiation was used: instead, the absorber temperature was fixed to a constant temperature to drive the convective flow inside the CPC. A similar setup was analysed using computational fluid dynamics (CFD). The resulting flow patterns, velocity magnitudes

Selection and/or peer review under responsibility of EuroSun2014 Scientific Committee
doi:10.18086/eurosun.2014.16.18 Available at http://proceedings.ises.org

and temperatures are driven by the important heat transfer mechanisms: conduction, convection and (internal) radiation. Transient calculations in 3D are required for a detailed reproduction of the natural convection currents. Being computationally cheaper - steady simulations in 2D lead to a reasonable overall agreement. The individual heat transfer mechanisms can be separated and the possible level of detail for a numerical CPC assessment is demonstrated. To investigate the influence of distributed energy sources on tube and mirror, ray-tracing techniques have been employed in the simulations for the CPC geometry. Section 2 will introduce both, a real CPC geometry and the lab scale geometry used for the comparative work. Here, we will also give an overview on the PIV measurements. Ray tracing will be described in section 3 applying the method for numerical assisted absorber tube positioning and tube-mirror contact area design. Furthermore, ray-tracing is a perfect visualization technique to assess the optical behaviour of a CPC. The numerical methods for heat transfer and fluid flow are introduced in section 4 and results for the flow patterns are compared to experimentally acquired data from the PIV measurements. In section 5 we will show the capability of the numerical methodology to clearly separate the different heat transfer mechanisms. In section 6 we will then use the CFD technique to calculate collector efficiencies for various scenarios including inert gas filling and the dependence on gravity and cavity pressure. Concluding remarks will be given in section 7.

2. Geometrical Setup and Experimental Methods

Particle Image Velocimetry (PIV) is used to visualize and quantify the typical flow patterns inside the CPC geometries. This methodology was applied to both a real sized collector (see section 2.1) and a lab scale collector (see section 2.2).

2.1. Real Geometry

Figure 1 (left) shows a PIV setup applied to a real sized collector in the solar simulator of AIT – the resulting seeding patterns visualizing the flow field are given in figure 1 (right). The images taken by the camera show strong reflections and also mirror images can be seen on the left and right lower corners of the image. These effects have to be treated accordingly in the data analysis.

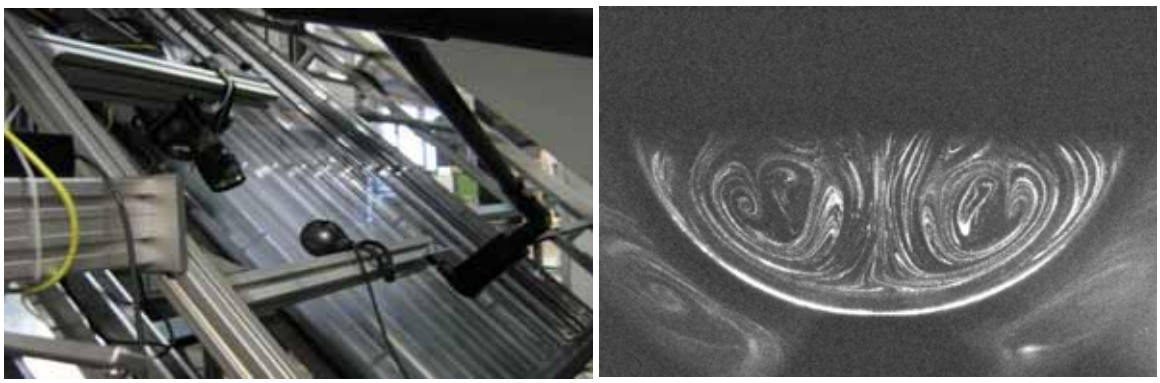

Fig. 1: (left) PIV setup mounted in front of a CPC collector in the solar simulator of AIT. (right) typical flow pattern visualized with proper seeding.

Whereas the PIV method has only been applied in the indoor test rig (see figure 1 (left)) for security reasons, collector efficiency measurements can also be performed on the outdoor tracker (see figure 2).

Fig. 2: Real geometry placed on the tracker for measurement of collector efficiency

2.2. Lab scale setup

A sketch in figure 3 illustrates the major components of the lab scale setup consisting of a double pulsed laser producing a laser light sheet and a camera capable of recording dual frames in short time intervals. Furthermore, temperature probes are mounted on the glass and mirror surfaces (see also figure 9 for temperature probe positions on the mirror (M) and on the glass (G)) to capture the local temperature variations.

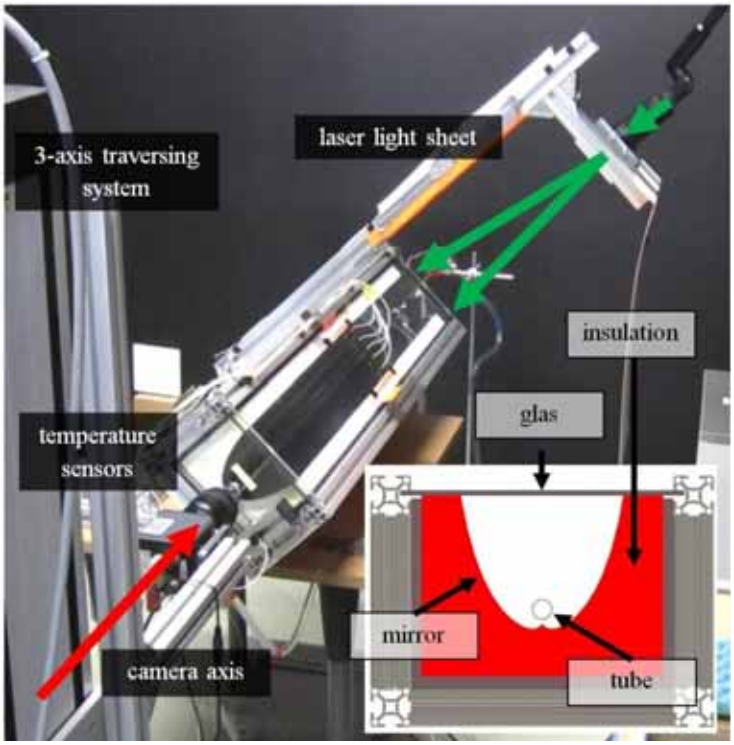

Fig. 3: Experimental setup and geometry; image of the PIV setup showing the lab scale CPC which can be tilted (45° setup shown here), the camera with camera axis (red arrow), the laser with laser light sheet plane (symbolized by two green arrows) perpendicular to the camera axis and the 3-axis traversing system for exact positioning of camera and laser; insert: cut through the lab scale CPC showing isolation (red), mirror, glass and tube

Whereas temperature data is readily available (for a comparison to numerical data see Reichl et. al. (2013)), a careful analysis had to be performed for the post processing of the PIV data. The cavity of the CPC is filled with a seeding, which follows the convective flow patterns triggered by the hot tube. Visualizing the

convective flow requires the choice of proper seeding and stabilization times to extract the governing convective patterns. A resulting flow pattern extracted out of a PIV series using data analysis based on cross correlation is shown in picture 7 right and discussed in section 4. The design for the truncated CPC initially was made for an absorber tube directly placed on the involute tip of the mirror. However, to avoid excessive thermal conduction between the absorber tube and the mirror, the tube was shifted upwards without changing the mirror geometry (see figure 3, insert). This of course changes the optical behaviour of the CPC. Therefore, ray-tracing techniques have been used to assess the changes (see figure 5) introduced.

3. Raytracing

Using the calculation methods of non-imaging optics (see for example Winston and Minano, 2005) and standard ray tracing techniques the optical design of a CPC collector (see e.g. Rabl (1976)) is straightforward. In this work, an in-house developed ray tracer (Kubicek et al. (2010), Popovac et al. (2010)) is used to visualize the ray distribution in CPC collectors. For a CPC geometry with a tube and fin absorber setup, figure 4 shows examples of typical ray families differing in the number of reflections and their way through the cavity.

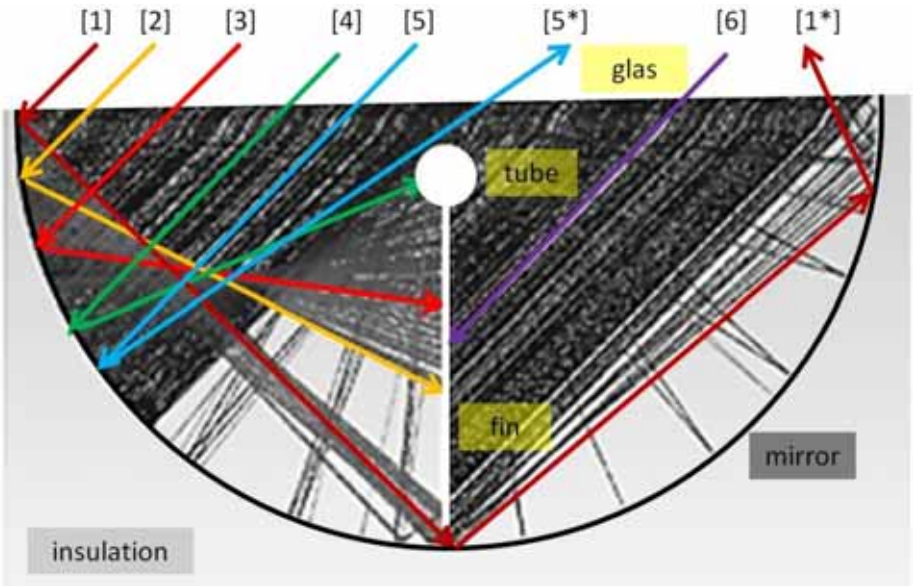

Fig. 4: Visualization of ray tracing results for an incoming ray angle of 45°. In the setup shown here, the receiver tube is positioned in the vicinity of the covering glass and connected to a vertical fin gathering the rays. Several types of rays can be distinguished [1]-[6] differing in the number of reflections and their way through the cavity. The slight dual refraction in the glass and some reflections are not shown for simplicity

Not all rays (e.g. [1] and [5]) can be captured by the absorber in this setup: To avoid heat conduction, a distance has to be kept between tube-glass and fin-mirror. Solar rays are lost (e.g. [1*] and [5*] through these gaps and thus do not contribute to the absorbed energy on the absorber. The ray tracing technique is – besides providing source terms for the CFD calculations – therefore a valuable tool for optimizing the cavity design of a CPC. In contrast to the tube-fin setup shown in figure 4, the setup used for comparing numerical (CFD) to experimental (PIV) data in the following section 4 is based on a truncated CPC design. For this setup without fin, ray tracing was used to quantify the sensitivity of the efficiency when moving the tube closer to the mirror (see figure 5) and to evaluate different local designs in the gap area between tube and mirror (see figure 6).

A larger distance between tube and mirror is preferable from a thermodynamically point of view, as heat conduction from the hot tube to the mirror leading to enhanced heat losses due to conduction should be avoided. Enlarging this gap, however, more rays are lost in this design thus reducing the efficiency. The

results given in figure 5 are based on reflectivity and absorptivity values set to 95% and show the dependency of the efficiency and a shift in acceptance angle when changing the tube – mirror distance – the outer geometry remains unchanged for these calculations. The changes in the acceptance angle by moving the tube in figure 5 are due to the fact, that the outer geometry of the CPC used for the shown ray tracing analysis has not been specifically designed for the presented varying absorber positions. A CPC, however, can be designed to include a gap between the absorber tube and the involute tip – this is done by using a virtual absorber based design. In that case, the outer geometry would be changed to account for the tube position. Thus, shifting the tube in the current design is equivalent to using the CPC outside its design conditions, which leads to the differences in efficiency compared to what would be expected for the ideal CPC.

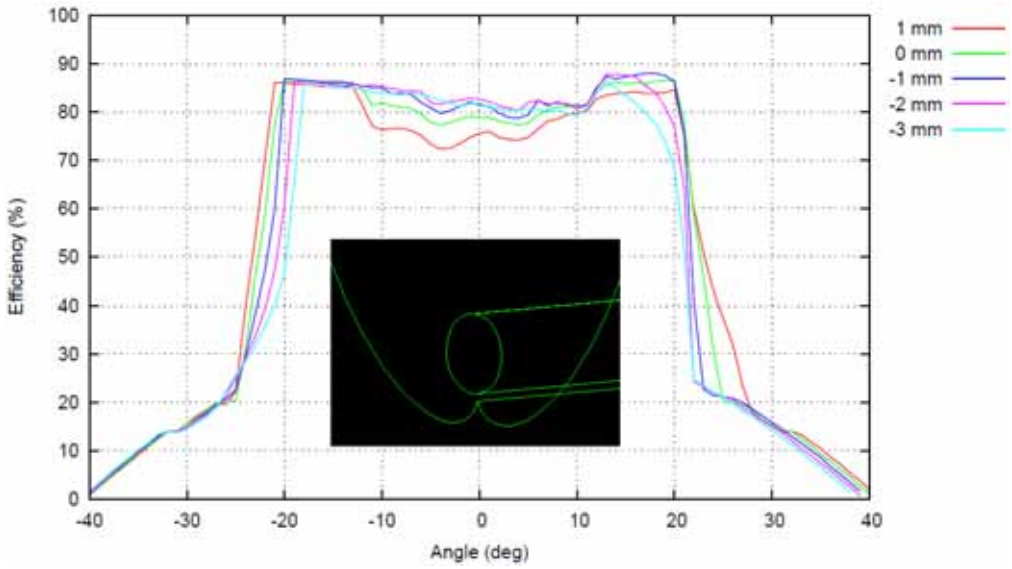

Fig. 5: Efficiency results based on ray tracing techniques for a typical CPC geometry while moving the absorber tube away from the mirror. The x-axis shows the angle of the incident rays. The different curves correspond to displacements of -3 (light blue), -2 (violet), -1 (dark blue), 0 (green), +1 mm (red) from the ideal position. The wavy-like curves are caused by using a restricted amount of rays; The diameter of the tube is 15 mm, reflectivity and absorptivity coefficients are 0.95.

Several designs of the contact area have been additionally tested by ray-tracing and their effect on efficiency is shown in figure 6 for visualization. While all designs show the same acceptance angle of approximately 20°, the zero angle efficiency is affected by the local design of the tube-mirror contact area.

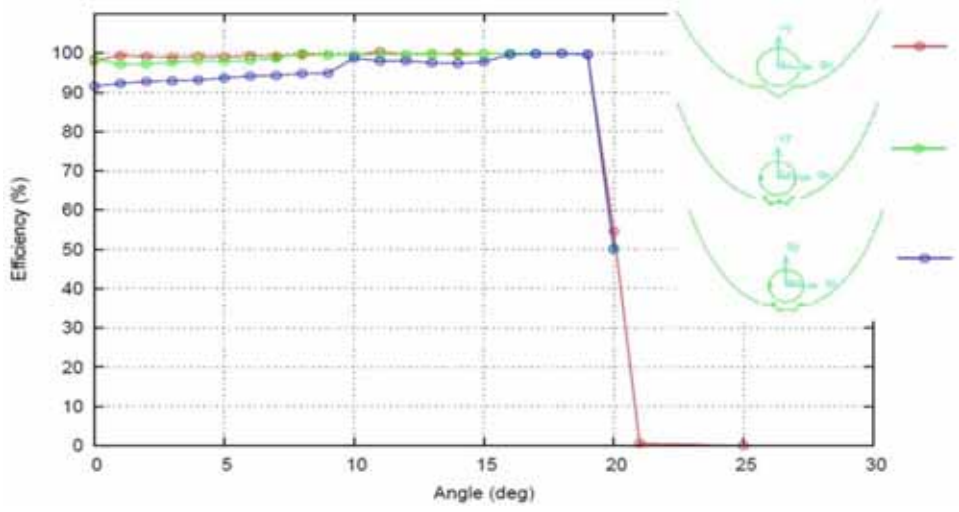

Fig. 6: Ray tracing results for different variants of the design of the tube-mirror contact area. The results have been calculated using an untruncated CPC geometry. The geometries on the right side from top to bottom correspond to the curve colours: red (top), green (mid), blue (bottom). Again, the x-axis shows the angle of incident rays. In these calculations a non-truncated CPC with an acceptance angle of 20° was used, reflectivity and absorptivity have been set to 100% and the tube absorber diameter is 15 mm.

Apart from visualization, quantitative analysis of ray tracing calculations provide the energy source terms necessary for complete coupled CFD simulations, which can provide tube water outlet temperatures solely based on geometry, material properties, incoming solar radiation, tube water inlet temperature and mass flow rate.

4. Numerical Method and Comparison to the experimental results

CFD has been applied both in 2D and 3D using steady and transient Navier Stokes solution techniques (ANSYS Fluent (ANSYS (2013))). The internal radiation effects have been captured by 'surface2surface' models. Heat conduction was made possible in all solid areas including mirror, tube, glass and mounting metals by introducing the necessary resolution in the numerical grids. The boundary conditions were chosen to mimic the lab scale experimental setup introduced in section 2.2: no incoming radiation was used and the tube temperature was kept at a fixed temperature. For a tilt angle of 45° figure 7 shows a comparison of typical flow patterns extracted from CFD (3D transient approach, left side) and PIV (right side).

A circulating flow (starting from the hot tube moving clockwise around the cavity along the (left) mirror (red up arrow), the glass and closing the loop on the opposite (right) mirror wall (blue down arrow)) can be seen. The yellow circle (top) marks an area where a small recirculation zone exists which is captured both in the experimental data (left figure 7) and in the numerical analogy (right figure 7). The blue circle (bottom) marks an area in the simulation which cannot be compared to experiment due to the lack of data in the optical shadow of the tube.

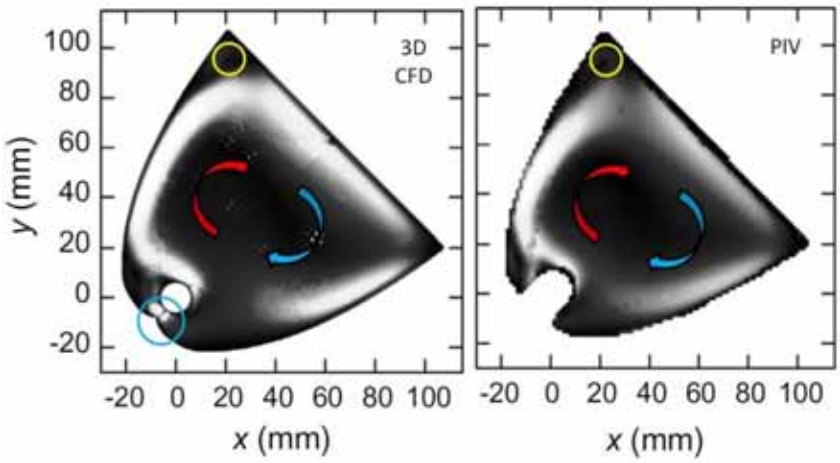

Fig. 7: Comparison of CFD (left) to PIV (right) – important flow features and velocity magnitudes (in-plane velocity magnitude in grey scale) are in good agreement. The velocity ranges from 0 to 10 cm/s.

Being computationally cheap, steady simulations in 2D lead to a reasonable overall agreement. Transient calculations in 3D, however, are required for a detailed reproduction of the natural convection currents (see Reichl et.al. for an elaborate discussion including temperature field comparisons for this setup).

The flow patterns and their stability largely depend on the tilt angle of the setup leading to a (unsteady) symmetric double circulation when no tilt is in place (similar to the patterns shown in figure 1 right). Figure 8 shows comparisons between CFD and PIV data for various tilt angles. The recirculation zone is increased in the numerical work in comparison to the PIV data, as the calculations have been performed in the faster 2D mode.

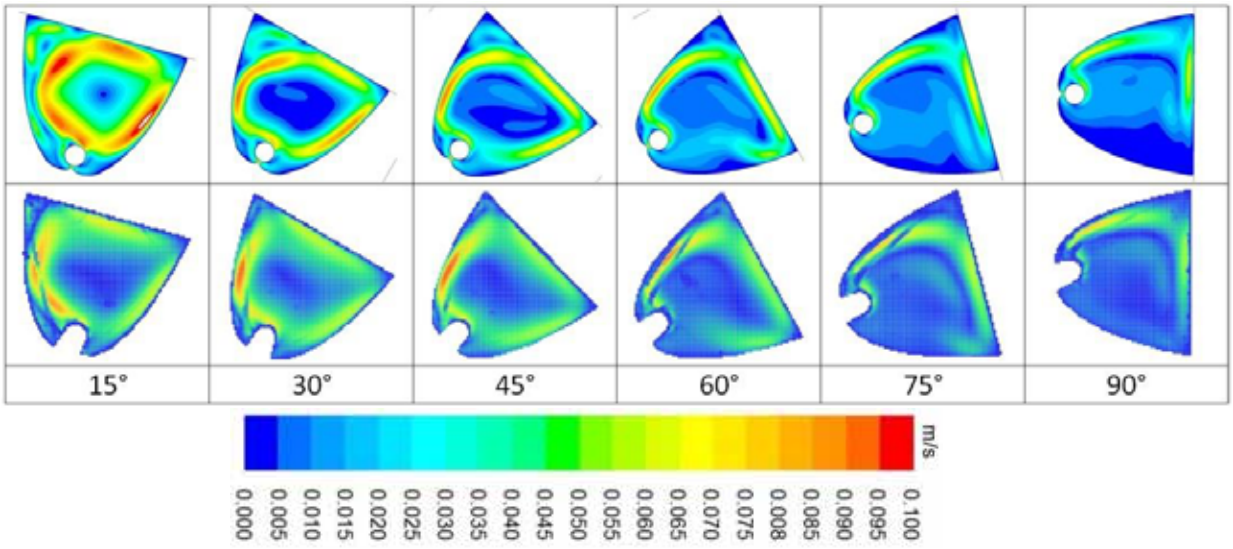

Fig. 8: Comparison of numerical CFD (*upper row*) to experimental PIV (*lower row*) contour plots of the in plane velocity magnitude for different angles of inclination. The gravitational force is always acting from top to bottom. Two dimensional simulations are not capable of reproducing all features of the flow especially at low inclination angles and in the areas of pronounced recirculation (range of in plane velocity magnitude approximately 0 – 0.1 m/s).

5. Separation of Heat Transfer Mechanisms

Separation of the individual heat transfer mechanisms (conduction, diffusion, convection and radiation) is possible by carefully analysing CFD simulations. Detailed heat flux distributions and local temperatures can be extracted. In most situations, only global parameters can be compared due to the lack of experimental data.

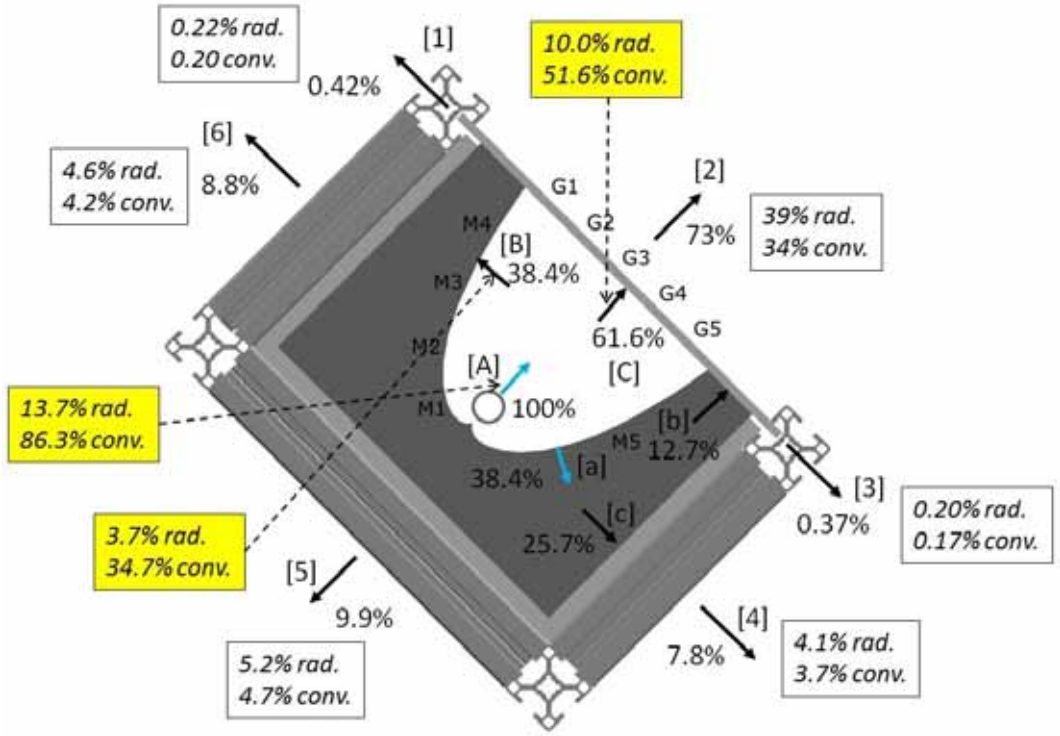

Fig. 9: Analysis of the different heat loss paths. They can be separated into the different heat transfer mechanisms (radiation, convection, conduction) – values are given in Table 1. The blue arrow [A] indicate the heat flux into the cavity (white region), the blue arrow [a] indicates the heat flux into the insulation (dark grey region).

For a 45°-tilted CPC (typical flow patterns can be seen in figure 8) a detailed heat flux analysis is shown in figure 9 and the corresponding temperature and heat flux values are given in table 1. Like the experiments shown in section 2, the tube is kept at a fixed temperature (79.2°C). At the tube the introduced heat flux is 100%. This energy is distributed to the outer walls (outer loop [1]-[6]) following the different heat transfer mechanisms (including radiation, conduction and convection). At the outer walls the energy is transferred to the surroundings via convection (conv.) and radiation (rad.). In the cavity (inner loop [A]-[C]) the ratio between radiation and convection heavily depends on the absorber emissivity. In this case, 62% of the total heat flux, which is introduced through the absorber tube into the cavity, is transferred to the glazing [C], 84% of this energy being transported by means of convection. In the insulation, heat conduction is the only available means of heat transfer (loop [a]-[c]). The heat is carried from the mirror to the outer walls and the glass.

Tab. 1: Temperatures and distribution of the heat transfer to its convective and radiative part. [1]-[6] form the outer loop which gives a total heat transfer of 100% provided by the tube. [A]-[C] form the inner heat transfer in the cavity, [a]-[c] the heat transfer in the insulation solid. Convective part (column 3) and radiative part (column 4) always sum up to the total heat transfer (column 2). The temperatures are the surface averaged mean temperatures of the corresponding part.

	Temperature	total heat transfer	convective part	radiative part
	[°C]	[%]	[%]	[%]
[1]	29.1	0.42	0.22	0.20
[2]	33.0	73	39	34
[3]	28.9	0.37	0.20	0.17
[4]	28.3	7.8	4.1	3.7
[5]	28.2	9.9	5.2	4.7
[6]	28.4	8.8	4.6	4.2
[A]	79.2	**100**	13.7	86.3
[B]	43.8	38.4	3.7	34.7
[C]	33.0	61.6	10.0	51.6
[a]	-	38.4	-	-
[b]	-	12.7	-	-
[c]	-	25.7	-	-

6. Efficiencies in different simulation scenarios

The developed CFD methodology was used to study several important scenarios. For these simulations the fast 2D steady calculation variant has been deployed, its applicability shown and discussed previously (Reichl et. al. (2013)). Efficiency curves are shown in figure 10 for several scenarios: introduction of temperature dependent material parameters, effects of radiation and gravity, reduced air pressure and filling the collector with an inert gas. All scenarios are compared to a reference setup.

The area of an ambient to tube temperature difference of 150°C is magnified in the insert of figure 10. The reachable efficiency largely depends on the scenario: Using fixed values at room temperature for the important material parameters (+) overestimate the efficiency as the introduction of temperature dependent material parameters (X) lead to slightly lower values of the efficiency. Zero gravity (□, ∨) and calculations without radiation (o) are only of theoretical interest. Evacuation down to p = 10 mbar (◊) of the absorber leads to the best efficiency followed by the filling with argon (∧).

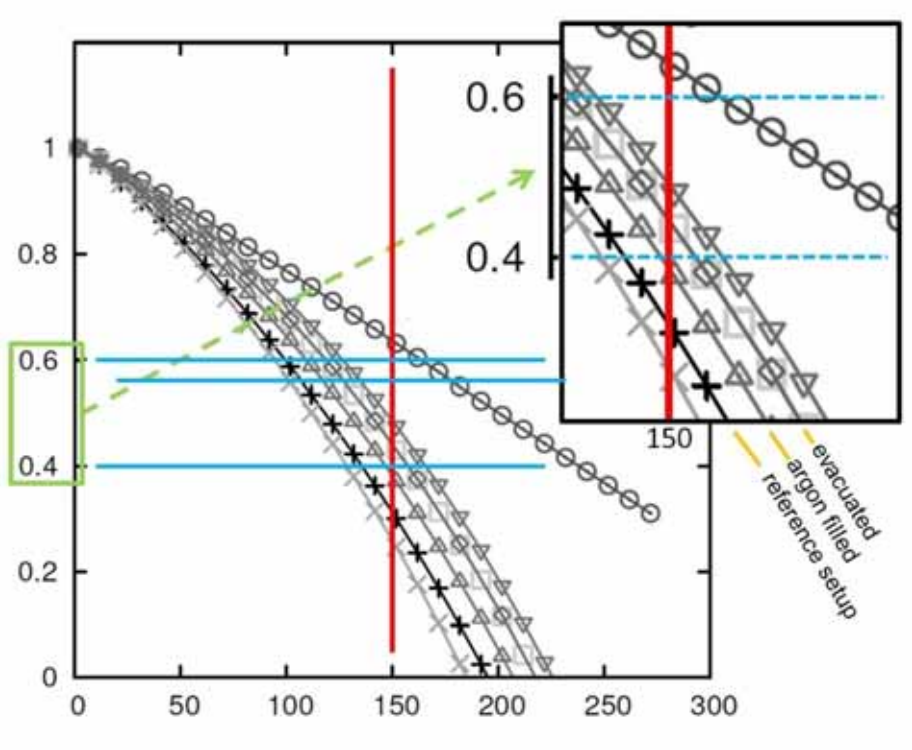

Fig. 10: Simulation results for the efficiencies for different scenarios: reference (+), temperature dependent material parameters (X), no radiation (o), zero gravity (□), argon filled (∧), argon filled and zero gravity (∨), p=10 mbar (◊). The x-axis shows the temperature difference between absorber and ambient; the y-axis shows the reached efficiency. The red line in the insert marks a temperature difference of 150°C. The orange lines indicate the important scenarios.

7. Conclusions

In this contribution we show the application of several experimental and numerical methodologies to the field of CPC collectors. Laser optical flow measurement techniques on both a real sized CPC and a lab scale setup have been performed. The flow patterns acquired by PIV are compared to CFD simulations for different tilt angles. 3D transient calculations are capable of reproducing all relevant flow features. The simulation techniques can be used to separate the individual heat transfer mechanisms, which are demonstrated for a reference setup showing the high level of detail available. Ray tracing techniques have been employed for the CPC geometry. This method can be used to quantify the energy source terms for the CFD simulations and to evaluate different mirror–tube arrangements and tube-mirror gap designs. Together with the heat transfer analysis provided by CFD these tools can be used to balance heat loss based on heat conduction and efficiency decrease due to loss of incoming rays. CFD methods can also be used to calculate efficiency curves for various material parameters, heat transfer coefficients, inert gas fillings and reduced pressures, which consequently make the introduced numerical methods a valuable tool set for collector design and prototype development.

8. Acknowledgements

The Austrian Research Promotion Agency (FFG) is gratefully acknowledged for funding this work under Grant No. 825522.

9. References

Abdel-Khalik, S.I., Li, H.-W., Randell, K.R., 1978. *Natural convection in compound parabolic concentrators – a finite element solution*. Journal of Heat Transfer 100, 199–204.

ANSYS, Inc., 2013. ANSYS, FLUENT, release 14.0.

Buttinger, F., Beikirchner, T., Pröll, M., Schölkopf, W., 2010. *Development of a new flat stationary evacuated CPC-collector for process heat applications*. Solar Energy 84, 1166–1174.

Chew, T., Tay, A., Wijeysundera, N., 1989. *A numerical study of the natural convection in CPC solar collector cavities with tubular absorbers*. Journal of Solar Energy Engineering 111, 16–23.

Eames, P.C., Norton, B., 2010. *Detailed parametric analyses of heat transfer in CPC solar energy collectors*. Solar Energy 50, 321–338.

Horta, P., Henriques, J.C.C., Collares-Pereira, M., 2012. *Impact of different internal convection control strategies in a non-evacuated CPC collector performance*. Solar Energy 86, 1232–1244.

Khonkar, H.E.I., Sayigh, A.A.M., 1995. *Optimization of the tubular absorber using a compound parabolic concentrator*. Renewable Energy 6 (1), 17–21.

Kubicek, B., Popovac, M., Frohner, A., Rudolph, M., Teppner, R.. 2010. *Fluent als Platform: ζ-f Turbulenzmodellierung und spectrales Path/Raytracing*, ANSYS Conference & CADFEM Austria Users Meeting, Wien, Österreich; 22.04.2010 - 23.04.2010; in: "www.usersmeeting.at", CADFEM Austria, (2010).

Popovac, M., Kubicek, B., Frohner, A., Semlitsch, B., 2010. *Path-tracing Approach for Solar Radiation Modeling in CFD*; EuroSun 2010 - International Conference on Solar Heating, Cooling and Buildings, Graz, Österreich; 28.09.2010 - 01.10.2010; in: "Proceedings EuroSun 2010 - International Conference on Solar Heating, Cooling and Buildings", (2010), Paper-Nr. 148.

Rabl, A., 1976. *Solar concentrators with maximal concentration for cylindrical absorbers*. Applied Optics 15 (7), 1871–1873.

Reichl, Ch., Hengstberger, F., Zauner, Ch., 2013. *Heat transfer mechanisms in a compound parabolic concentrator: Comparison of computational fluid dynamics simulations to particle image velocimetry and local temperature measurements*. Solar Energy 97, 436-446.

Singh, H., Eames, P.C., 2011. *A review of natural convection heat transfer correlations in rectangular cross-section cavities and their potential applications of compound parabolic concentrating (CPC) solar collector cavities*. Applied Thermal Engineering 31, 2186–2196.

Winston, R., Minano, J.C., 2005. *Nonimaging Optics*. Elsevier Academic Press.